OMAE2018-77072

ANALYTICAL FORMULATION OF NONLINEAR FROUDE-KRYLOV FORCES FOR SURGING-HEAVING-PITCHING POINT ABSORBERS

Giuseppe Giorgi[*]
Centre for Ocean Energy Research
NUI Maynooth
Maynooth, Co. Kildare, Ireland
Email: giuseppe.giorgi.2015@mumail.ie

John V. Ringwood
Centre for Ocean Energy Research
NUI Maynooth
Maynooth, Co. Kildare, Ireland
Email: john.ringwood@mu.ie

ABSTRACT

Accurate and computationally efficient mathematical models are fundamental for designing, optimizing, and controlling wave energy converters. Wave energy devices are likely to exhibit significant nonlinear behaviour, over their full operational envelope, so that nonlinear models may become indispensable.

Froude-Krylov nonlinearities are of great importance in point absorbers but, in general, their calculation requires an often unacceptable increase in model complexity and computational time. However, if the body is assumed to be axisymmetric, it is possible to describe the whole geometry analytically, thereby allowing faster calculation of nonlinear Froude-Krylov forces.

In this paper, a convenient parametrization of axisymmetric body geometries is proposed, applicable to devices moving in surge, heave, and pitch. In general, the Froude-Krylov integrals must be solved numerically. Assuming small pitch angles, it is possible to further simplify the problem, and achieve an algebraic solution, which is considerably faster than numerical integration.

NOMENCLATURE

p Pressure.
γ Specific weight of the sea water.
η Free surface elevation.
$a = \frac{H_w}{2}$ Wave amplitude.
$\omega = \frac{2\pi}{T_w}$ Wave frequency.

$\chi = \frac{2\pi}{\lambda}$ Wave number.
h Water depth.
$S(t)$ Instantaneous wetted surface.
$\mathbf{F}_g$ Gravity force.
WEC   Wave energy converter.
FK   Froude-Krylov.
LFK   *Linear* method for computing FK forces.
VFK   Algebraic nonlinear FK forces with *vertical* coordinates.
RFK   Numerical nonlinear FK forces with *rotating* coordinates.

1 INTRODUCTION

Mathematical models are indispensable for designing, optimizing, and controlling wave energy converters (WECs). Ideally, such models are required to be both accurate and computationally efficient. The most popular models are linear, which are convenient for their short computation time, but accurate only for small relative fluid/body motions. Conversely, wave energy converters are likely to experience large movements, especially under controlled conditions, in order to maximize the power absorption. Consequently, significant nonlinear effects may arise, so that linear models become less reliable [1].

The inclusion of nonlinear terms in the equation of motion may improve the accuracy of the model, but with additional complexity and computational burden. In particular, it has been shown, in the literature, that nonlinear Froude-Krylov (FK) forces, which are the integral of the static and dynamic pressure over the wetted surface of the device, are especially important

---

[*]Address all correspondence to this author.

for point absorbers [2]. Furthermore, nonlinear FK forces are responsible for purely-nonlinear phenomena, such as pitching instability or parametric roll [3].

For geometries of arbitrary complexity, the computation of nonlinear FK forces first requires the discretization of the surface with a mesh, and then the employment of a time-consuming remeshing routine, at each time step, in order to calculate the instantaneous wetted surface of the device [4]. However, if the body is assumed to be axisymmetric, it is possible to describe the complete geometry analytically, thereby avoiding the use of a mesh [5]. Note that such a hypothesis is not particularly restrictive, since the vast majority, if not the totality, of point absorbers are designed to be non-directional, and are therefore axisymmetric. Due to the analytical description of the geometry, the computation of nonlinear FK forces is considerably faster than the meshing approach.

In this paper, a convenient parametrization of axisymmetric surfaces is proposed, applicable to devices moving in three degrees of freedom, allowing an analytical description of nonlinear FK forces in surge, heave, and pitch. In general, the FK integrals must be solved numerically using, for example, a trapezoidal rule. Assuming small pitch angles, it is possible to further simplify the problem, and achieve an algebraic solution, which is considerably faster than numerical integration. Hereafter, LFK is used as the acronym for *linear* FK force, VFK for the algebraic-nonlinear model (since it assumes a *vertical* geometry), and RFK for the numerical-nonlinear model (since it considers a *rotating* geometry).

The application of these three different approaches to the FK force calculation (linear, algebraic-nonlinear, and numerical-nonlinear) may depend on the particular purpose the mathematical model is intended for. For preliminary studies, shape optimization, or WEC farm configuration analysis, many iterations are required; therefore, the requirement for fast calculation prevails over the accuracy requirement. In case of power production assessment, or control optimization routines, a higher level of accuracy is of great importance, at a significantly low computational time; therefore, the algebraic-nonlinear approach may be the most appropriate. Finally, higher degree of accuracy is needed in order to compute maximum loads (for the design of the mechanical properties of the structure and mooring lines), or for verifying the likelihood of events such as instability or parametric roll. In such cases, the numerical-nonlinear method may be preferred.

However, the choice between the LFK, VFK, and RFK, strongly depends on the operational space spanned by the device in its operating conditions, in particular the heave displacement and the pitch angle. In fact, for small motions, linear assumptions are reasonably valid, and all models effectively overlap. Conversely, when the device experiences large motions, typically induced by the control strategy, important differences between the models may arise.

The purpose of this paper is to provide a simple and computationally convenient formulation for nonlinear FK forces for axisymmetric wave energy converters, moving in surge, heave, and pitch. A case study is then considered, inspired by the CorPower device [6], in order to quantify differences in accuracy and computation time for linear, algebraic-nonlinear and numerical-nonlinear models. The remainder of the paper is organized as follows: Sect. 2 presents the different methods to compute FK forces, which are validated in Sect. 3. Some results and discussions are presented in Sect. 4, and final remarks and conclusions are given in Sect. 5.

2 FROUDE-KRYLOV FORCE

In the framework of linear potential theory, FK forces correspond to the integral of the pressure of the undisturbed wave field over the wetted surface of the device. Such a pressure is defined, according to linear Airy's theory, as:

$$p(x,z,t) = p_{st} + p_{dy} = -\gamma z + \gamma a \frac{\cosh\left(\chi\left(z+h\right)\right)}{\cosh\left(\chi h\right)} \cos\left(\omega t - \chi x + \varphi\right) \tag{1}$$

where $p_{st} = -\gamma z$ is the static pressure, p_{dy} the dynamic pressure, γ the specific weight of the sea water, a the wave amplitude, χ the wave number, ω the wave frequency, φ an arbitrary phase (usually set to zero), h the water depth, defined according to a right-handed inertial frame of reference $Oxyz$, with the origin at the still water level (SWL), x pointing in the direction of propagation of the wave, and z pointing upwards. The free surface elevation η is defined as

$$\eta(x,t) = a\cos\left(\omega t - \chi x + \varphi\right) \tag{2}$$

Note that, for the irregular wave case, p_{dy} and η are defined as superposition of different frequency components, so that the method, described in this paper for regular waves, is straightforward to generalize to irregular waves, as shown in [7]. Froude-Krylov forces are computed by integrating the pressure, shown in equation (1), over the instantaneous wetted surface $S(t)$. In particular, static and dynamic FK force components can be defined, respectively, as follows:

$$\mathbf{F}_{FK_s} = \mathbf{F}_g + \iint\limits_{S(t)} -\gamma z \mathbf{n} dS \tag{3a}$$

$$\mathbf{F}_{FK_d} = \iint\limits_{S(t)} p_{dy} \mathbf{n} dS \tag{3b}$$

TABLE 1: SUMMARY OF THE MAIN DIFFERENCES BETWEEN THE THREE FROUDE-KRYLOV MODELLING APPROACHES FOR AXISYMMETRIC BUOYS.

	LFK Linear Froude-Krylov (FK)	**VFK** Algebraic nonlinear FK	**RFK** Numerical nonlinear FK
Wetted surface $S(t)$	Constant	Instantaneous	Instantaneous
Pitch angle δ	0	0	δ
Free surface $\eta(x,t)$	0	$\eta(t)$	$\eta(x,t)$
Computational time	+	++	+++
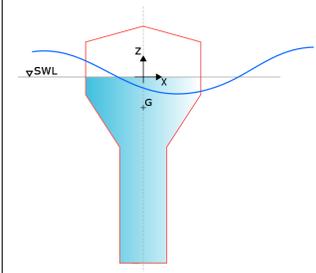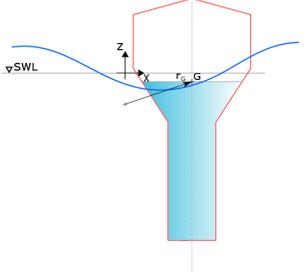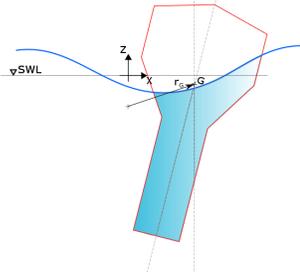
where $\mathbf{n} = (n_x, n_y, n_z)$ is the unit vector normal to the surface, pointing outwards, and $\mathbf{F}_g$ is the gravity force. Likewise, FK torques are defined as follows:

$$\mathbf{T}_{FK_s} = \mathbf{r} \times \mathbf{F}_g + \iint\limits_{S(t)} -\gamma z \mathbf{r} \times \mathbf{n} dS \qquad (4a)$$

$$\mathbf{T}_{FK_d} = \iint\limits_{S(t)} p_{dy} \mathbf{r} \times \mathbf{n} dS \qquad (4b)$$

where $\mathbf{r}$ is the position vector, defined as (x,y,z), and $\times$ is the cross product.

For a geometry of arbitrary complexity, it is not possible to solve the FK integrals, from (3a) to (4b). Linear boundary-element solvers linearize the problem around the still water level (SWL: $z = \eta = 0$), therefore considering a constant wetted surface.

Alternatively, the geometry can be discretized through a mesh, computing the contribution to the force over each mesh panel [4]. Such an approach is computationally expensive, due to the recalculation, at each time step, of the instantaneous wetted surface, and consequent remeshing of the geometry. For *axisymmetric* buoys, a convenient parametrization of the wetted surface can ease the calculation of the FK integrals. In particular, computationally efficient algebraic solutions of the FK integrals exist for vertical axisymmetric buoys [5]. Such a method is further described in Sect. 2.2.

If the body is pitching as well, numerical integration is required. Such a method is further described in Sect. 2.1. Table 1 summarises the main different characteristics of LFK, VFK, and RFK, highlighting different assumptions and, qualitatively, different computational time requirements. Quantitative accuracy and computational time comparisons are presented in Sects. 3 and 4.

2.1 Nonlinear Froude-Krylov Force: Algebraic Integration

Both the algebraic (VFK) and the numerical (RFK) integration approaches rely on the assumption of axisymmetric geometry, which allows the analytical description of the whole wetted surface. The geometry of a generic axisymmetric buoy with vertical axis can be described in cylindrical coordinates, as follows:
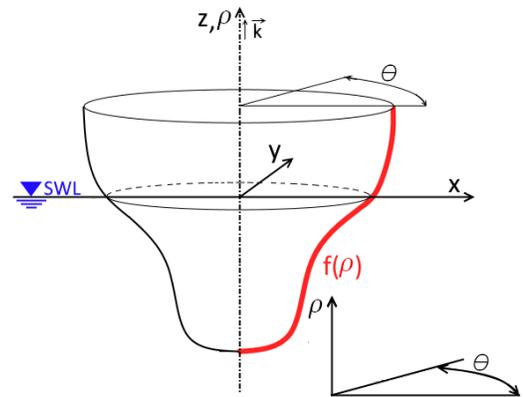

FIGURE 1: AXISYMMETRIC VERTICAL DEVICE WITH GENERIC PROFILE OF REVOLUTION $f(\rho)$.

$$\begin{cases} x(\rho,\theta) = x_G + f(\rho)\cos\theta \\ y(\rho,\theta) = f(\rho)\sin\theta \\ z(\rho,\theta) = z_G + \rho \end{cases}, \quad \theta \in [-\pi,\pi) \wedge \rho \in [\rho_1,\rho_2]$$

$$(5)$$

where $f(\rho)$ is a generic function of the vertical coordinate ρ, describing the profile of revolution of the axisymmetric body, as shown in Fig. 1. The centre of gravity (*CoG*) which, at rest, is assumed to lie on the axis at $(0,0,z_{CoG})$, moves about the $x-$ and $z-$ axis of x_G and z_G, respectively.

The change of coordinates, from the Cartesian (x,y,z) to the cylindrical (ρ,θ), requires the inclusion of $\|\mathbf{e}_\rho \times \mathbf{e}_\theta\|$ in the integral, where $\mathbf{e}_\rho$ and $\mathbf{e}_\theta$ are unity vectors in the ρ and θ directions, respectively. Furthermore, $\mathbf{n}$ can be expressed as $\frac{\mathbf{e}_\rho \times \mathbf{e}_\theta}{\|\mathbf{e}_\rho \times \mathbf{e}_\theta\|}$. Simplifying the denominator of $\mathbf{n}$, it follows that the integral in (3b), for example, becomes:

$$\mathbf{F}_{FK_d} = \iint\limits_{S(t)} p_{dy}(x,y,z)\mathbf{n}dS = \int\limits_{\theta_1}^{\theta_2}\int\limits_{\rho_1}^{\rho_2} p_{dy}(\rho,\theta)\left(\mathbf{e}_\rho \times \mathbf{e}_\theta\right)d\rho\,d\theta$$

$$(6)$$

The cross product of the unity vectors is defined as follows:

$$\mathbf{e}_\rho \times \mathbf{e}_\theta = \begin{pmatrix} f'(\rho)\cos\theta \\ f'(\rho)\sin\theta \\ 1 \end{pmatrix} \times \begin{pmatrix} -f(\rho)\sin\theta \\ f(\rho)\cos\theta \\ 0 \end{pmatrix} = f(\rho)\begin{pmatrix} -\cos\theta \\ -\sin\theta \\ f'(\rho) \end{pmatrix}$$

$$(7)$$

Likewise, for the torque integrals:

$$\mathbf{r} \times \left(\mathbf{e}_\rho \times \mathbf{e}_\theta\right) = \begin{pmatrix} f(\rho)\cos\theta \\ f(\rho)\sin\theta \\ \rho \end{pmatrix} \times f(\rho)\begin{pmatrix} -\cos\theta \\ -\sin\theta \\ f'(\rho) \end{pmatrix}$$

$$(8)$$

The integral in (6) can be algebraically solved, for a vertical axisymmetric buoy, only if ρ_2 (the top limit of integration) is horizontal. Therefore, ρ_2 is set constant, and equal to the free surface elevation at the axis of the buoy. Such a condition is quite accurate if the wave length is much longer than the characteristic horizontal dimension of the device at the free surface elevation, which is often the case. Finally, note that, for the computation of nonlinear FK forces, it is advantageous to apply Wheeler stretching to the dynamic pressure in equation (1) [7].

2.2 Nonlinear Froude-Krylov Force: Numerical Integration

The analytical description of the rotated axisymmetric body, pitching at an angle δ about an axis parallel to the y-axis, and passing through $CoG = (x_G, 0, z_{CoG} + z_G)$, can be obtained by applying a rigid rotation matrix to the vertical coordinate system in (5), giving:

$$\begin{cases} x(\hat\rho,\theta) = f(\frac{\hat\rho}{\cos\delta})\cos\theta\cos\delta + \hat\rho\tan\delta - z_{CoG}\sin\delta + x_G \\ y(\hat\rho,\theta) = f(\frac{\hat\rho}{\cos\delta})\sin\theta \\ z(\hat\rho,\theta) = -f(\frac{\hat\rho}{\cos\delta})\cos\theta\sin\delta + \hat\rho + z_{CoG}(1-\cos\delta) + z_G \end{cases}$$

$$(9)$$

where $\hat\rho$ is a temporary parameter, which will be substituted shortly, in order to solve the following problem: with the current formulation of $z(\hat\rho,\theta)$, it is not straightforward (or possible, in some cases) to extract the value of the integral limits, $\hat\rho_1$ or $\hat\rho_2$, in order to satisfy an arbitrary condition $z(\hat\rho,\theta) = z^*$. In particular, it is impossible to define the value of the top limit $\hat\rho_2$ such that $z^* = \eta = a\cos\left(\omega t - \chi x(\hat\rho,\theta) + \varphi\right)$.

It is therefore convenient to re-parametrize the surface, using a new parameter, such that $z(\rho,\theta) = \rho$, so that any arbitrary conditions can be easily imposed, just as $\rho_2 = z^*$. By applying the substitution $z = \rho$ in (9), the new coordinate system is defined, as follows:

$$\begin{cases} x(\rho,\theta) = f(\frac{h(\rho,\theta)}{\cos\delta})\cos\theta\cos\delta + h(\rho,\theta)\tan\delta - z_{CoG}\sin\delta + x_G \\ y(\rho,\theta) = f(\frac{h(\rho,\theta)}{\cos\delta})\sin\theta \\ z(\rho,\theta) = \rho \end{cases}$$

$$(10)$$

where $h(\rho,\theta)$ is a functional depending on the particular geometry. Typical examples are given:

- Cylinder, with $f(\rho) = R$:
  $h(\rho,\theta) = \rho + R\cos\theta\sin\delta + z_{CoG}(\cos\delta - 1)$
- Cone, with $f(\rho) = m\rho + q$:
  $h(\rho,\theta) = \frac{\rho - z_G + q\cos\theta\sin\delta + z_{CoG}(\cos\delta - 1)}{1 - m\cos\theta\tan\delta}$

Using equation (10), the unity vectors $\mathbf{e}_\rho$ and $\mathbf{e}_\theta$ can be calculated, and the nonlinear FK integrals can be defined. Such integrals must be solved numerically using, for example, a trapezoidal rule. The computational time depends on the numerical scheme utilized, and on the relative and absolute tolerances used to approximate the integral, which have been set to 0.1 and 100, respectively, based on the numerical value of the expected forces and on a sensitivity analysis. Furthermore, it is convenient to compute the static and dynamic FK forces together, in order to reduce the number of integrals to be solved. Finally, we can note that computing the integral with the coordinate system in (10) is faster than using the coordinates in (9).
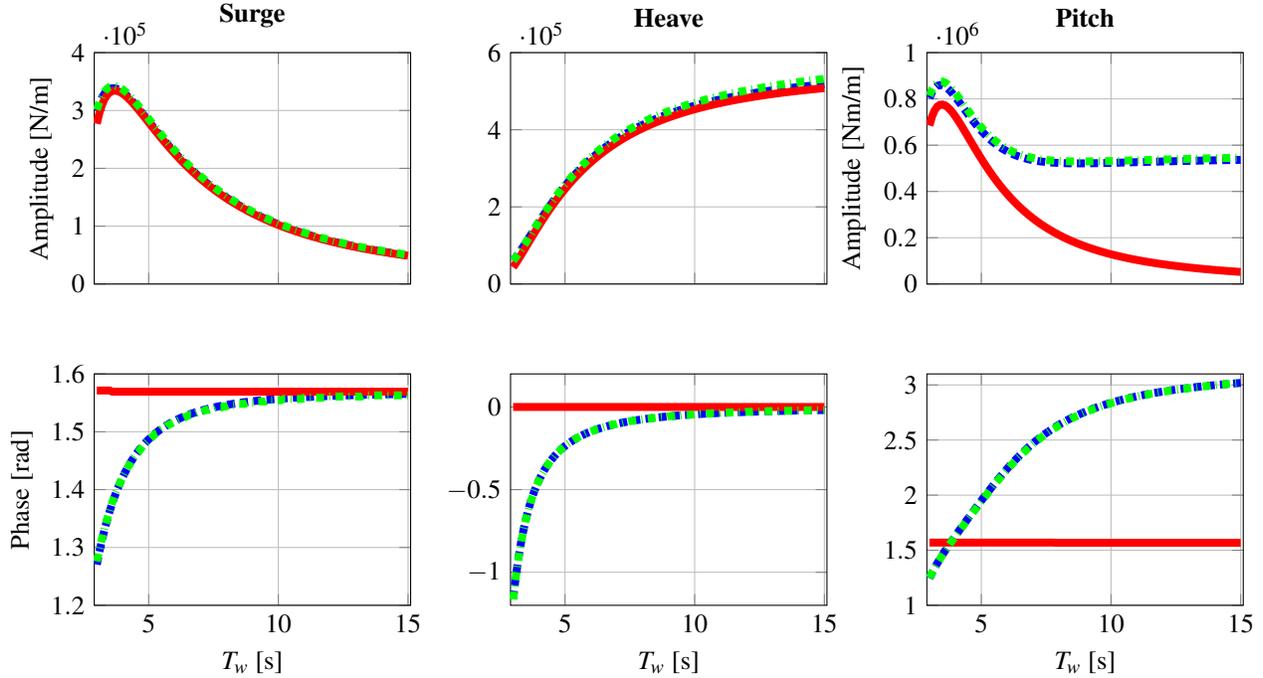
4

FIGURE 2: VALIDATION, IN LINEAR CONDITIONS, OF THE RFK METHOD (━ ▪ ▪ ━), COMPARED WITH LINEAR RESULTS FOR THE CORPOWER BUOY ROTATED BY 15° (▪▪▪▪). FOR COMPARISON, THE VFK METHOD IS PRESENTED (━━), WHICH REFERS TO A VERTICAL BUOY.

Eventually, the actual value of the computational time depends on the complexity of the geometry. Indeed, real buoys may be a combination of different sections, typically cylinders and cones, as in the case shown in Table 1. Each section of the buoy requires an individual integral. For the CorPower geometry, which is described in Sect. 3, it is found that the numerical integration scheme is, on average, about 80 times slower than the algebraic integration, where the computational time of the VFK method is of the order of magnitude of 10^{-4}s. However, it is important to point out that all the calculations are performed in Matlab, which is between one and two orders of magnitude slower than lower level coding languages [8].

3 VALIDATION

Several checks have been performed, in order to ensure the code to be correct and reliable. The surface of several simple geometries, generated with either the vertical or the rotated cylindrical coordinates, has been visually inspected, with particular care on the ability to correctly represent the intersection between the rotated buoy and the free surface elevation. All the algebraic calculations have been checked via the symbolic calculation software Wolfram Mathematica [9], and effectively compared with numerical integration. Furthermore, surface and volume integrals have been computed, in order to calculate the surface and volume of sample geometries (cylinders and cones), either vertical or rotated.

Linear boundary element (BEM) codes can be used to validate the static and dynamic FK integrals; using very small motions and wave amplitudes, the nonlinear models should overlap with linear results. Hereafter, a particular device is taken into account for the computation of FK forces, based on the CorPower device [6], whose shape is shown in Table 1. Based on [10], the device specifications are shown in Fig. 3.

The BEM code WAMIT [11] is used to calculate the linear surge, heave, and pitch hydrodynamic stiffness and the linear dynamic FK force for the vertical device. The nonlinear static FK forces are calculated with the VFK and RFK method, using very small displacements, 0.01m and 0.01rad, while the nonlinear dynamic FK forces are computed with waves of different periods T_w, and height $H_w = 0.01$m. The three models (LFK, VFK, and RFK) return the very same results, validating the method in linear conditions. Note that, in general, the RFK method converges to the VFK method when the pitch angle is zero.

A second configuration is run in WAMIT, considering the geometry statically rotated by 15° around its centre of gravity, in order to compute the hydrostatic stiffness and FK force linearized around a non-zero pitch angle, and validate the RFK method for a rotated geometry. Figure 2 shows the validation of the dynamic
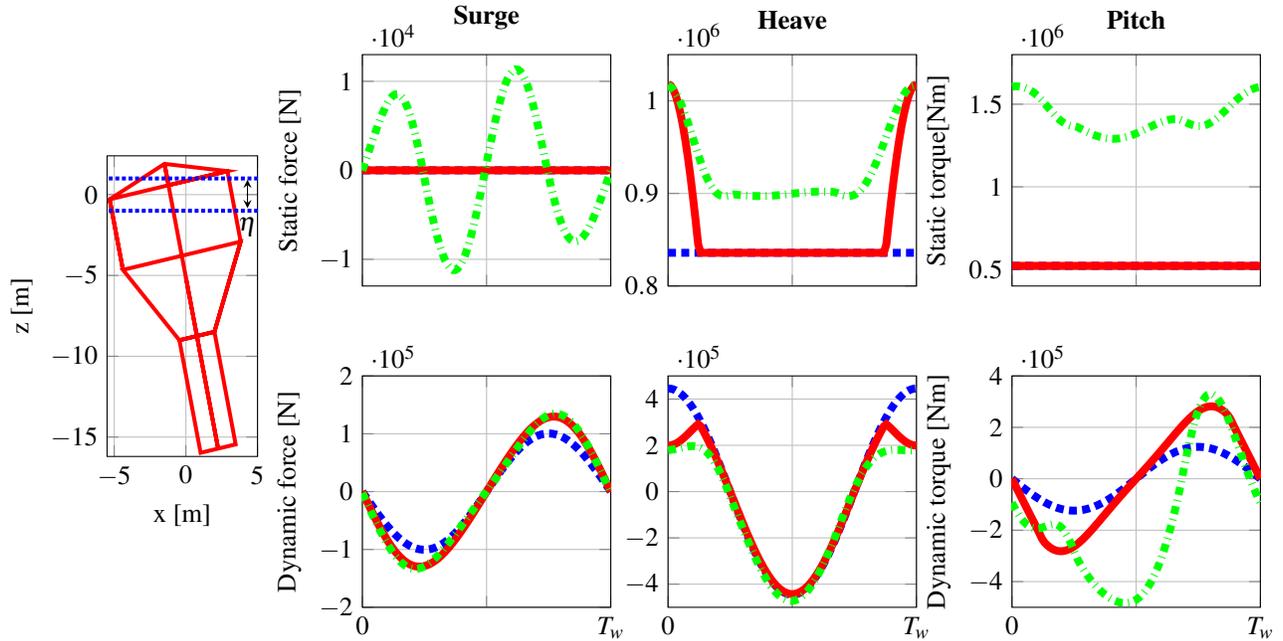
FIGURE 4: FK FORCES FOR THE CORPOWER BUOY, FIXED AT $z_G = -1.5$m AND $\delta = -15°$, AS SHOWN IN THE FIGURE ON THE LEFT, SUBJECT TO A WAVE WITH $H_w = 2$m AND $T_w = 10$s, ACCORDING TO LFK (▪▪▪▪), VFK (▬▬), AND RFK (▪▪▪▪).
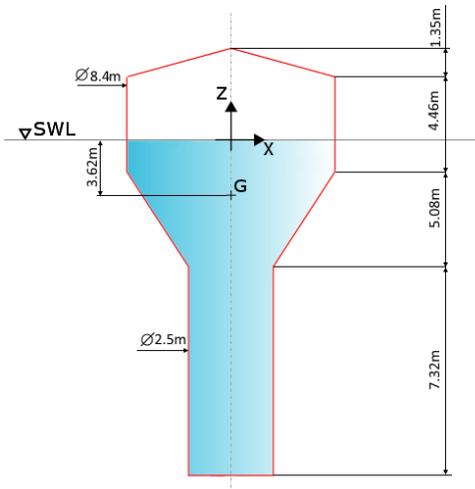

FIGURE 3: SHAPE AND DIMENSIONS OF THE CASE STUDY BUOY, INSPIRED BY THE CORPOWER DEVICE.

FK force amplitude coefficients and phase lags, with respect to the free surface elevation.

On the one hand, the LFK and RFK models are almost perfectly overlapping, both for the amplitude and phase. The slight differences are due to an approximation that the BEM code in-

troduces, due to the meshed geometry, as supposed to the actual analytical geometry, considered in RFK. On the other hand, the VFK curve describes the dynamic forces for the vertical geometry instead. From the comparison between VFK and RFK, it is interesting to notice that there is a phase difference in all three degrees of freedom. While the phase is constant for the vertical buoy (VFK), it is frequency-dependent for the rotated one (RFK).

Furthermore, it can be noted that the amplitudes of surge and heave are the almost the same, while are significantly different for the pitch torque. Such a difference can be explained considering which translation forces (surge and/or heave) contribute to the formation of the pitch torque: for a vertical buoy, the heave forces have, overall, no contribution to the torque, due to the axisymmetric geometry. In fact, the pitch profile has the same shape of the surge one. Conversely, for a rotated buoy, both surge and heave contribute to the pitch torque, which resembles the profile of the surge curve at low periods (large surge, small heave), and vice versa at high periods (small surge, large heave). Similar considerations can be seen for the phase lags.

4 RESULTS AND DISCUSSION

The relative disparity in accuracy between the three methods (LFK, VFK, and RFK) depends on four different factors: two concerning the position of the device (z_G and δ), and two concerning the wave characteristics (H_w and T_w). Therefore, regular waves are considered, in order to study the specific dependence

6

on H_w and T_w. Most importantly, higher waves induce larger variations in the wetted surface during the wave cycle, inducing more significant nonlinearities. On the other hand, the LFK and VFK methods converge for small values of z_G; similarly, VFK and RFK converge for small values of δ. Given the typical oscillatory response of a WEC, differences between models vanish in that part of the response cycle corresponding to a zero crossing, while they are maximal at the peaks and troughs of the oscillation.

In order to understand how linear and nonlinear models vary and differ from each other, and how they depend on z_G and δ, surge, heave, and pitch, static and dynamic FK forces are computed, for several different regular waves, having *fixed* the device in a particular position. An example of the such forces is presented in Fig. 4. The following ranges are considered: $T_w \in [4s, 15s]$, with 1s step; $H_w \in [0.5m, 3m]$, with 0.5m step; $z_G \in [-3m, 3m]$, with 0.25m step; $\delta \in [-15°, 15°]$, with 1.5° step. Static and dynamic FK forces are examined in Sects. 4.1 and 4.2, respectively.

4.1 Static Froude-Krylov forces

The static surge FK force (F_{st}^s) is zero for both LFK and VFK since, for a vertical buoy, regardless the instantaneous wetted surface, static pressure contributions at diametrically opposite points cancel out. Note that, in the case of VFK, such a result is the consequence of the flat surface elevation assumption. Indeed, using the RFK model for a vertical buoy would return a non-zero F_{st}^s, since the actual (not flattened) free surface is considered.

For a rotated geometry, F_{st}^s is non-zero since part of the geometry pierces the water and, therefore, does not have a diametrically opposite point. In particular, it can be noted, from Fig. 4, that the frequency of F_{st}^s is about twice the wave frequency. In fact, F_{st}^s is zero twice as often as η is zero: firstly, when η has its peak/trough on the buoy axis, so that p_{st} is symmetric with respect to the $y-z$ plane; secondly, when η is zero on the buoy axis, so that p_{st} is symmetric with respect to the $x-y$ axis. In both cases, the contributions from diametrically opposite points cancel out. However, such variations have small importance, since the static surge FK force is always one or two orders of magnitudes smaller than the heave force.

As shown in Fig. 4, the static heave FK force (F_{st}^h) is linear, for the VFK model, when η intersects the cylinder section, while becoming nonlinear in the cone section, since the cross sectional area is not constant. A more general representation on how F_{st}^h varies can be achieved using an "equivalent" stiffness, where F_{st}^h is divided by z_G. Figure 5 shows such an equivalent stiffness for a particular wave, at $\delta = 15°$, and varying z_G. Results for the nonlinear VFK and RFK models are represented by areas, since F_{st}^h is not constant.

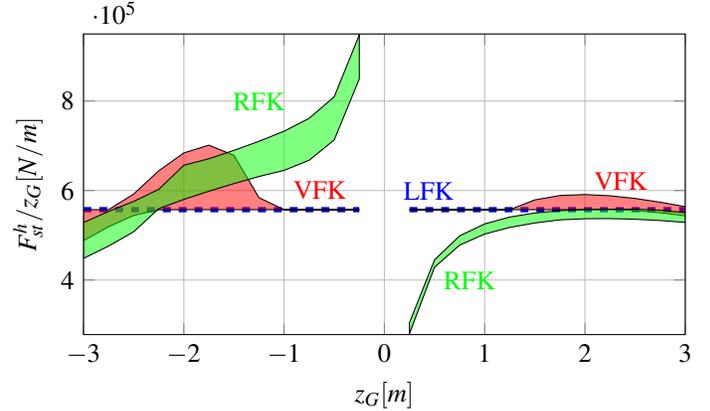The VFK model coincides with the LFK for small vertical

FIGURE 5: EQUIVALENT STATIC HEAVE FROUDE-KRYLOV FORCE FOR THE CORPOWER BUOY, ROTATED OF $\delta = -15°$, SUBJECT TO A WAVE WITH $H_w = 2m$ AND $T_w = 10s$, ACCORDING TO LFK (▪▪▪), VFK (▬), AND RFK (▬).

displacements, since η intersects the buoy only at the cylinder section, while differences are found at larger z_G. Conversely, RFK is always nonlinear, since the actual rotated geometry is considered. Note that a larger equivalent stiffness for small z_G does not mean a larger error; in fact, the difference appears larger just because F_{st}^h is divided by a smaller z_G.

The nonlinearity/variability of F_{st}^h, for both the VFK and RFK models, depends on which buoy section is engaged by η. In particular, larger errors are introduced by the top cone (engaged when z_G is large and negative), which has a more pronounced slope than the bottom cone (engaged when z_G is large and positive), since the rate of change of the cross sectional area of the top cone is greater. Note that similar graphs can be drawn for different T_w and H_w. While the equivalent heave stiffness is largely insensitive to the wave period, larger wave heights introduce larger errors, since larger changes of the wetted surface appear.

Finally, the static pitch FK torque (F_{st}^p) is considered. Figure 6 presents F_{st}^p for different z_G and δ, for a sample wave of $T_w = 10s$ and $H_w = 2m$. Only positive pitch angles are shown, since results are symmetric. Given the variability of nonlinear F_{st}^p, as shown in Fig. 4, the mean torque is presented, along with error bars, whose length is equal to the standard deviation of the static torque, over one wave period. Overall, the variability is quite small, compared to the mean values, apart from a very negative z_G, where the highly nonlinear top cone intersects η.

Obviously, the RFK model significantly overlaps with the LFK model for very small z_G, and diverges from it with when the absolute value of either δ or z_G increases. Furthermore, for vertical displacements larger than 1.75m, the static torque changes sign, contributing to drive the buoy away from the equilibrium position, as opposed to acting as a restoring torque, which is the
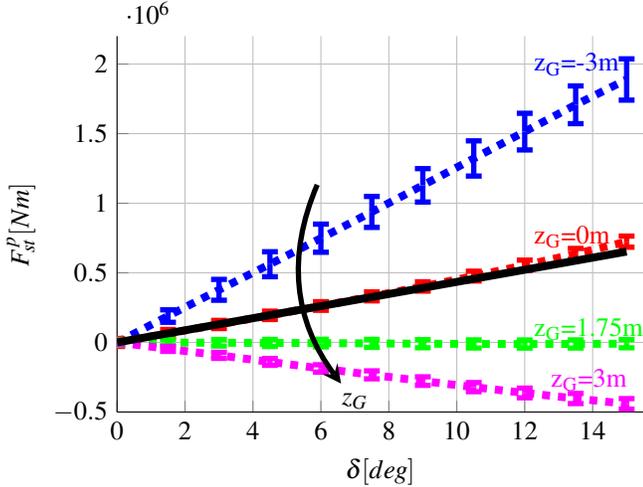
FIGURE 6: STATIC PITCH FROUDE-KRYLOV FORCE FOR THE CORPOWER BUOY, SUBJECT TO A WAVE WITH $H_w = 2m$ AND $T_w = 10s$, ACCORDING TO LFK AND VFK (SOLID LINE), AND RFK (DASHED LINE), FOR DIFFERENT z_G.

case in a linear model.

Finally, as in Fig. 5, Fig. 6 shows a significantly insensitivity of F_{st}^p to T_w, while larger values of H_w cause slightly smaller absolute mean values of F_{st}^p, and slightly increased variability.

4.2 Dynamic Froude-Krylov forces

In order to discuss differences between the three models in calculating dynamic FK forces, the normalized root mean squared error (NRMSE) is used. Such an error is computed with respect to the RFK model, which is effectively retained as the benchmark. The normalization is performed with respect to the maximum absolute value of either the torque, for the pitch torque, or the magnitude of the vectorial sum of surge and heave, for surge and heave forces. In this way, the error of each linear force component is weighted with its impact on the total force (namely errors on surge are less important than errors on heave, since the heave force is typically much larger than the surge one). Results are shown in Fig. 7 and 8.

Indeed, it can be seen that errors in surge are smaller than those in heave and pitch. Figure 7 shows that the VFK model is much better than the LFK model, especially for larger z_G, and is largely symmetric with respect to z_G. However, there is small influence of δ. Figure 8 shows that errors increase at smaller T_w, mainly due to the phase difference discussed in Sect. 3, and shown in Fig. 2. Furthermore, the surge error becomes more relevant, at small T_w, because the surge force increases for shorter waves. Indeed, since the surge force depends more on the wave length than the wave height, the error is less sensitive to H_w.

With reference to the dynamic FK force in heave, shown

in Fig. 7, it can be noted that the VFK model is much better than the LFK model for negative z_G (where the top cone is engaged), while quite similar errors are evident for small or positive z_G (where either the cylindre or the bottom cone are engaged). Considering Fig. 8, similarly to the surge errors, heave errors increase at smaller T_w, mainly due to larger phase difference (see Fig. 2). Moreover, larger errors are found at larger H_w, since the wave height is the main driver of the heave force.

Finally, errors in pitch torque, in Fig. 7, are large for almost all z_G and δ, apart from very small pitch angles, for both the LFK and VFK models. However, both in Fig. 7 and Fig. 8, the VFK model is better than the LFK model.

5 CONCLUSION

This paper discusses the importance and relevance of nonlinear Froude-Krylov force representation for axisymmetric wave energy converters, moving in surge, heave, and pitch. The assumption of an axisymmetric device makes the analytical description of the surface of the device possible, therefore avoiding the use of time-consuming mesh-based approaches. In particular, two computationally convenient methods are proposed: one using a numerical integration scheme, the other algebraically solving the Froude-Krylov integrals, relying on the assumption of small pitch angles.

As a case study, the CorPower wave energy device is considered. After validation, a parametric study is performed, in order to discuss the accuracy and differences between different models. Overall, it is found that significant nonlinearities in surge and heave appear when the fluid intersects the conical sections of the buoy, therefore mainly depending on the heave position z_G, and the wave height H_w. However, nonlinearities in surge, even though they are present, seem to be of little relevance, due to their smaller amplitude, compared to heave FK forces. On the contrary, nonlinearities in pitch appear to be important for a wide range of device positions (z_G and δ) and waves (T_w and H_w).

In order to discuss the true importance of nonlinear effects, the response of the WEC must be considered, so that the effective dynamics of the system are taken into account, and only the actual operational space of the device is investigated. Future work will deal with the simulation of the WEC response, subject to regular and irregular waves, and depending on different control strategies, which are likely to enhance nonlinear effects.

Furthermore, as future work, it should be possible to build a hybrid nonlinear Froude-Krylov model to compute each force with an appropriate model, in order to achieve a homogeneous level of accuracy. As an example, one plausible option is to use a linear model for surge, an algebraic-nonlinear model for heave, and a numerical-nonlinear model for pitch. The objective is to define a parsimonious model, which achieves the best compromise of accuracy and speed, focusing the computational effort only where needed.
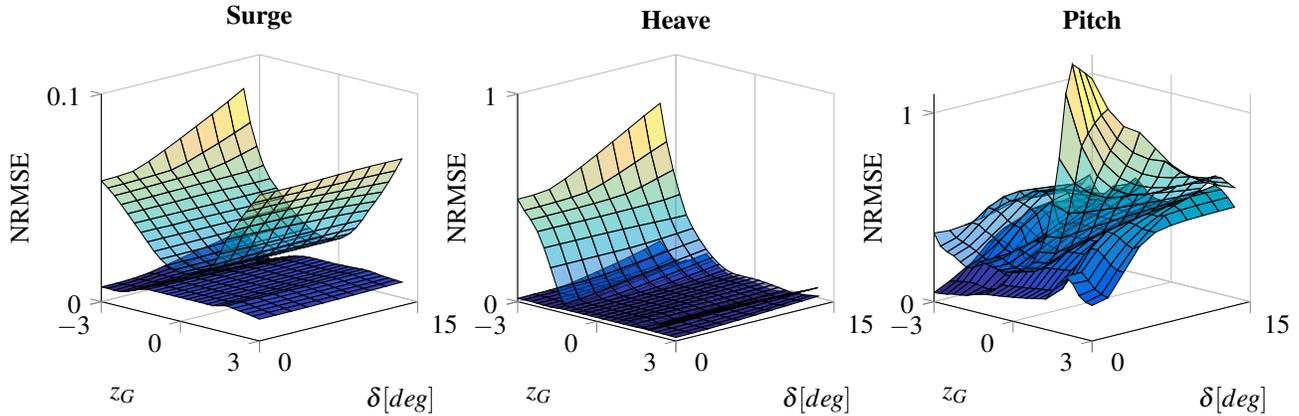
FIGURE 7: NORMALIZED ROOT MEAN SQUARE ERROR FOR DYNAMIC FROUDE-KRYLOV FORCES, WITH A WAVE OF $T_w = 10s$ AND $H_w = 2m$. THE TOP SEMI-TRANSPARENT SURFACE CORRESPONDS TO LFK, WHILE THE BOTTOM OPAQUE SURFACE CORRESPONDS TO VFK
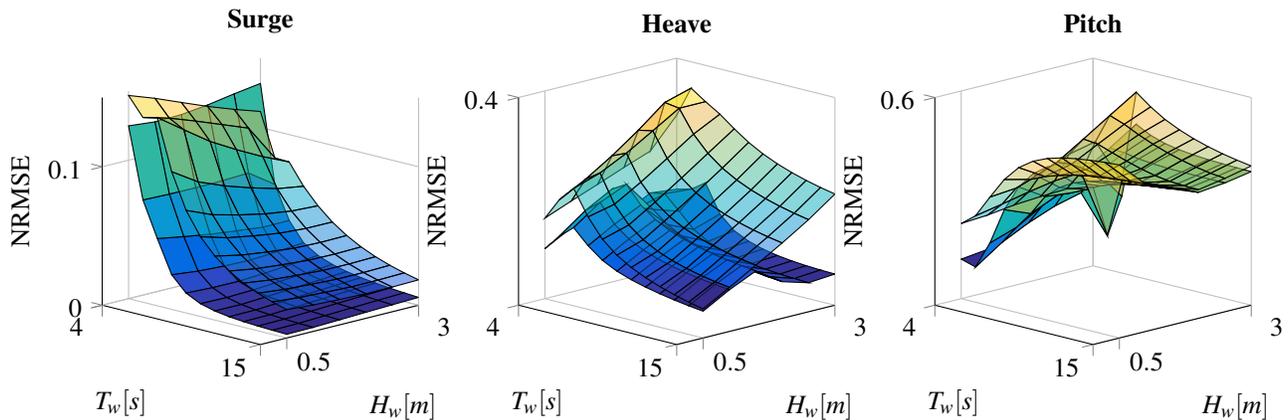

FIGURE 8: NORMALIZED ROOT MEAN SQUARE ERROR FOR DYNAMIC FROUDE-KRYLOV FORCES, AT $z_G = -1.5m$ AND $\delta = 15°$. THE TOP SEMI-TRANSPARENT SURFACE CORRESPONDS TO LFK, WHILE THE BOTTOM OPAQUE SURFACE CORRESPONDS TO VFK

REFERENCES

[1] Giorgi, G., and Ringwood, J. V., 2017. "Froude-krylov and viscous drag representations in nonlinear wave energy devices models in the computation/fidelity continuum". *Ocean Engineering, 141*, pp. 164–175.

[2] Giorgi, G., and Ringwood, J. V., 2017. "Comparing nonlinear hydrodynamic forces in heaving point absorbers and oscillating wave surge converters". *Journal of Ocean Engineering and Marine Energy, 4*(1), pp. 25–35.

[3] Tarrant, K. R., 2015. "Numerical modelling of paramtetric resonace of a heaving point absorber wave energy converter". PhD thesis, Department of Mechanical & Manufacturing Engineering, Trinity College, March.

[4] Gilloteaux, J.-C., 2007. "Mouvements de grande amplitude d'un corps flottant en fluide parfait. application à la récupération de l'énergie des vagues.". PhD thesis, Ecole Centrale de Nantes-ECN.

[5] Giorgi, G., and Ringwood, J. V., 2017. "Computationally efficient nonlinear froude–krylov force calculations for heaving axisymmetric wave energy point absorbers". *Journal of Ocean Engineering and Marine Energy, 3*(1), pp. 21–33.

[6] CorPower, 2017. Corpower ocean ab, available at

http://www.corpowerocean.com/.

[7] Giorgi, G., and Ringwood, J. V., 2018. "Relevance of pressure field accuracy for nonlinear froude-krylov force calculations for wave energy devices". *Journal of Ocean Engineering and Marine Energy,* **4**(1), pp. 57–71.

[8] Wendt, F. F., Yu, Y.-H., Nielsen, K., Ruehl, K., Bunnik, T., Touzon, I., Nam, B. W., Kim, J. S., Kim, K.-H., Janson, C. E., et al., 2017. "International energy agency ocean energy systems task 10 wave energy converter modeling verification and validation". In 12th European Wave and Tidal Energy ConferencEuropean Wave and Tidal Energy Conference, Technical Committee of the European Wave and Tidal Energy Conference.

[9] Wolfram, 2017. Wolfram mathematica, available at http://www.wolfram.com/matavailable.

[10] Todalshaug, J. H., Asgeirsson, G. S., Hjálmarsson, E., Maillet, J., Möller, P., Pires, P., Guérinel, M., and Lopes, M., 2016. "Tank testing of an inherently phase-controlled wave energy converter". *International Journal of Marine Energy,* **15**, pp. 68–84.

[11] Inc., W., 2013. *WAMIT v7.0 manual*.